K-MM radiative-Auger transition rates for argon

V. O. Kostroun and G. B. Baptista*

Ward Reactor Laboratory, School of Applied and Engineering Physics, Cornell University, Ithaca, New York 14853

We present the results of the first calculation of the spectral distribution of emitted photons following K-MM radiative-Auger transitions in the free argon atom. The calculation is based on second-order perturbation theory, and the total transition rate found to be $2.68 \times 10^{-4}/\hbar$ eV, or 4% of the calculated $K\beta_{1,3}$ rate of $6.7 \times 10^{-3}/\hbar$ eV. The calculated rate and photon spectrum agree fairly well with the experimental data of Keski-Rahkonen and Utriainen. Difficulties which preclude a direct comparison between theory and experiment are discussed, especially the effects of the spectrometer response function on the experimental data. The need for more high-resolution data is emphasized.

I. INTRODUCTION

The radiative-Auger process is thought to be responsible for some of the observed structure on the low-energy side of ordinary x-ray emission lines.[1-6] In this process, the filling of an inner-shell vacancy by a less tightly bound electron is accompanied by the simultaneous emission of a photon and excitation of another electron into a bound or continuum level of the atom.

Thus far, two calculations of the *total* transition rate for the radiative-Auger process have been presented, but none of the partial rates into the possible different final states of the system or the detailed spectral distribution of the emitted photons. Bloch,[7] who first postulated the existence of the radiative-Auger process in order to explain the continuum observed by Bloch and Ross on the low-energy side of the $K\beta_5$ of molybdenum,[1] estimated on the basis of Richtmyer's double-jump theory[8] the total radiative-Auger transition rate for the special case where such transitions replace dipole forbidden transitions. More recently, Åberg[6] has shown that the simultaneous emission of an x-ray photon and electron can accompany dipole allowed transitions as well, and attributes the process to the change in the average potential acting on the electrons in the atom when the inner-shell vacancy moves to an outer shell (shakeoff), and to the interaction between single- and double-hole configurations in the final state (configuration interaction).

In this paper we present the first detailed calculation of the spectral distribution of photons emitted in the radiative-Auger process. The calculated spectrum is for the K-MM radiative-Auger transition in the argon atom, and the total rate is obtained by summing over the individual transition rates. In our approach, we explicitly treat the atom and the radiation field as one system, and consider transitions from one state of the atom to another due to the interaction between the two systems. This is the usual way of dealing with the familiar radiation processes such as emission and absorption. While the calculation of the transition rate for these processes is carried out to first order in perturbation theory, the calculations of transition rates of more complicated radiation processes, e.g., scattering of a photon by an electron, or processes involving more than one photon, etc., require higher orders in perturbation theory and proceed via intermediate or virtual states.[9] We consider the radiative-Auger process an example of a more complicated radiation process, and calculate its transition rate in second-order perturbation theory.

II. THEORY

A. Previous approaches and calculations

Thus far, two calculations of the *total* transition rate for the radiative-Auger process have been presented. The first was developed by Bloch,[7] and although it was only an estimate of the order of magnitude of the effect, we discuss it in some detail to show that it is in a sense a forerunner of the present and Åberg's[6] calculations. The estimate was based on Richtmyer's double-jump theory,[8] which attributed the existence of x-ray satellites to the simultaneous transition of *two* electrons in doubly ionized atoms produced in the initial excitation process. Bloch considered the radiative-Auger process in two steps, treating the creation and filling of the two vacancies separately. The calculated transition rate was given by the product of the probability for the simultaneous ejection of an outer-shell electron from an atom owing to the sudden removal of an inner-shell electron, and the probability of a simultaneous transition, accompanied by the emission of

a photon, of two interacting electrons to the two unoccupied levels (inner- and outer-shell vacancy). The initial and final states of the two electrons undergoing the transition were taken as

$$\psi_i = u_\alpha(1)u_a(2) + \sum_{\mu,m}^{UO} \frac{\langle \mu m |v| \alpha a \rangle}{\epsilon_\mu + \epsilon_m - \epsilon_\alpha - \epsilon_\alpha} u_\mu(1)u_m(2)$$

and $\psi_f = u_\beta(1)u_b(2)$, where u_ρ is the unperturbed single-particle state of the atom with corresponding single-particle energy ϵ_ρ and the sum is over unoccupied states. The probability that an outer electron is excited following the creation of an inner-shell vacancy was given by

$$\epsilon = 1 - \left| \int u_b^{Z+1} u_b^Z \, d\tau \right|^2,$$

where u_b^{Z+1} and u_b^Z are single-particle states in an atom with nuclear charge $Z+1$ and Z, respectively. The radiative-Auger rate W_{fi} was then estimated from

$$W_{fi} = \frac{2\pi}{\hbar} |M|^2 \frac{g\epsilon}{g\epsilon + 1 - \epsilon} \rho(E_f),$$

where g is the number of equivalent electrons occupying level b, $\rho(E_f)$ is the density of final states available to the ejected photon and electron, and $M = \langle \psi_f | (e/mc)\vec{p}_1 \cdot \vec{A}(\vec{r}_1) | \psi_i \rangle$ is the matrix element for the process. No detailed calculations were presented, and only an estimate of the total radiative-Auger rate was given for the special case where such transitions replace dipole forbidden transitions.

Apart from calculational details (e.g., the Coulomb potential $v = e^2/r_{12}$ was expanded in only a few terms in one of the electron's coordinates and all exchange terms were neglected), Bloch's expression for the radiative-Auger rate is very similar to the the the one that would be obtained if the effect were treated as a polyelectron phenomenon and the rate calculated in the sudden approximation.[10,11]

This brings us to the only other, more complete calculation of the total radiative-Auger rate, based directly on the sudden approximation and developed by Åberg.[6] The basic idea of Åberg's approach is that the orbitals of all the electrons in the atom rearrange as a result of the change in the average potential acting on the electrons when the x-ray hole moves from the inner to the outer shell and gives rise to photon emission. Those bound electrons which have velocities small compared to the propagating hole suffer a "sudden" perturbation due to the change in the screening of the nuclear charge and may undergo transitions to excited states.

Specifically, Åberg considers double electron

transitions accompanied by photon emission in which an outer-shell electron in orbit nl jumps to an inner-shell vacancy $n_0 l_0$ and another outer-shell electron in orbit $n'l'$ is simultaneously excited into a bound or continuum state $\epsilon \bar{l}$ [Fig. 1(c)]. The energy of the emitted photon is $\hbar\omega = I_{n_0 l_0} - I_{nl, n'l'} - \epsilon$, where $I_{n_0 l_0}$ is the $n_0 l_0$ ionization energy of the neutral atom and $I_{nl, n'l'}$ is the energy of the simultaneous ionization of the two electrons nl and $n'l'$ from the neutral atom. Separate self-consistent-field (SCF) equations are solved for the initial $(n_0 l_0)^{-1}$ single-hole state and for both the single-hole $(nl)^{-1}$ and double-hole configuration $[(nl)^{-1}(n'l')^{-1}]\epsilon\bar{l}$ final states. The final state is taken as a linear combination of both single- and double-vacancy states, i.e.,

$$\Psi_f = \phi_1 U_{1f} + \sum_{i \geq 2} \phi_i U_{ij},$$

where the functions ϕ_1 and ϕ_i as well as the initial-state wave function are Slater determinants built up from separate SCF orbitals. The spontaneous dipole transition rate between initial and final states of the atom is then evaluated. In atomic units, this rate is[6]

$$A_{if} = \tfrac{4}{3} \alpha^3 g_i^{-1} E_{if}^3 S_{if}, \tag{1}$$

where α is the fine-structure constant, g_i is the degeneracy of the initial level, and $E_{if} = E_i - E_f$ is the energy of the emitted photon. S_{if} is given by

$$\sum_{a,b} \left| \left\langle b \left| \sum_{j=1}^{N} \vec{r}_j \right| a \right\rangle \right|^2,$$

and the summation is carried out over the degenerate initial and final states a and b. The dipole matrix element in S_{if} gives rise to two terms (in the lowest nonvanishing order in both overlap elements $\langle n_2 l_2 | n_1 l_1 \rangle$ and mixing coefficients U_{ij})
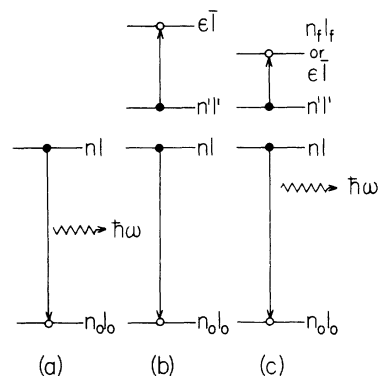

FIG. 1. Schematic representation of (a) radiative, (b) nonradiative or Auger, and (c) radiative-Auger processes, illustrating the notation used to designate quantum numbers that characterize the states of interest.

so that both shakeoff and configuration interaction in the final state give first-order contributions to the radiative-Auger transition probability, with the corresponding transition amplitudes either adding or subtracting. The calculated probabilities $A(K\text{-}L^2)$ and $A(K\text{-}M^2)$ of x-ray emission accompanied by simultaneous excitation of an electron to any of the excited $\epsilon p(s)$ states are divided, respectively, by the transition probability of the normal $(1s)^{-1} \to (2p)^{-1}$ and $(1s)^{-1} \to (3p)^{-1}$ x-ray lines to give the relative shakeoff probabilities $P(K\text{-}L^2)$ and $P(K\text{-}M^2)$, which are then calculated for a number of elements. In this calculation it follows directly that radiative-Auger transitions can accompany allowed dipole x-ray transition.

B. Present approach

We consider an N-electron atom (atomic number Z) with an inner-shell vacancy already created and the radiation field as one system. The Hamiltonian for this system (neglecting the usual $\vec{L} \cdot \vec{S}$, A^2, etc. terms) is given by

$$H = \sum_{i=1}^{N} \left(-\frac{\hbar^2}{2m} \nabla_i^2 - \frac{Ze^2}{r_i} \right) + \sum_{i<j}^{N} \frac{e^2}{r_{ij}} + H_{\text{rad}} + \sum_{i=1}^{N} \mathcal{K}_i(\vec{A}) ,$$

$$(2)$$

where the first two terms in the Hamiltonian describe the atom, H_{rad} is the free radiation field, and the last term gives the interaction between the atomic electrons and the radiation field, i.e.,

$$\sum_{i=1}^{N} \mathcal{K}_i(\vec{A}) = \sum_{i=1}^{N} \frac{e}{2mc} [\vec{p}_i \cdot \vec{A}(\vec{r}_i) + \vec{A}(\vec{r}_i) \cdot \vec{p}_i] . \quad (3)$$

We assume that an N-electron single-particle separable Hamiltonian approximates the atom

$$H_{\text{atom}} = \sum_{i=1}^{N} \left(-\frac{\hbar^2}{2m} \nabla_i^2 - \frac{Ze^2}{r_i} + V^N(r_i) \right) , \quad (4)$$

and hence Eq. (2) can be written as $H = H_{\text{atom}} + H_{\text{rad}} + H_I$, where H_I, the perturbing Hamiltonian for the system, is given by

$$H_I = \sum_{i<j}^{N} \frac{e^2}{r_{ij}} - \sum_{i=N}^{N} V^N(r_i) + \sum_{i=1}^{N} \mathcal{K}_i(\vec{A}) , \quad (5)$$

and where $V^N(r_i)$ is some (as yet unspecified) central field. The unperturbed wave functions of the system $H_{\text{atom}} + H_{\text{rad}}$ are a product of an N-particle wave function describing the state of the atom and a function describing the free radiation field. The wave functions of the free radiation field are given by[9]

$$\Psi(t) = e^{-iEt/\hbar} \prod_{\omega} \psi_{n_\omega} = e^{-iEt/\hbar} \psi_{\cdots n_\omega \cdots} ,$$

and are characterized by the number of photons n_ω, each of a given energy, polarization, etc.

present in the field. The total energy E of the radiation field is $E = \sum_\omega n_\omega \hbar \omega$.

The many-particle states of the atom which is approximated by the model Hamiltonian (4) can be represented by Slater determinants constructed from the solutions $\phi_{n_i l_i m_i s_i}(\vec{r}_i, \vec{\sigma}_i)$ of the single-particle Hamiltonian

$$\left(-\frac{\hbar^2}{2m} \nabla_i^2 - \frac{Ze^2}{r_i} + V^N(r_i) \right) \phi_{n_i l_i m_i s_i}(\vec{r}_i, \vec{\sigma}_i)$$

$$= \epsilon_{n_i l_i} \phi_{n_i l_i m_i s_i}(\vec{r}_i, \vec{\sigma}_i) , \quad (6)$$

where the $\epsilon_{n_i l_i}$ denote the single-particle energies. The Slater determinant is given by

$$\Phi_{k_1 \cdots k_N}(\vec{r}_1 \vec{\sigma}_1, \ldots, \vec{r}_N \vec{\sigma}_N) = \mathcal{Q}(\phi_{k_1}(1) \cdots \phi_{k_N}(N)) , \quad (7)$$

where $\mathcal{Q}$ is the antisymmetrization operator $\mathcal{Q} = (1/\sqrt{N!}) \sum_P (-1)^P P.$[12] In Eq. (7), the set of single-particle quantum numbers $n_i l_i m_i s_i$ of an electron with position and spin coordinates $\vec{r}_i \vec{\sigma}_i$ is denoted by k_i, and $\vec{r}_i \vec{\sigma}_i$ by (i), and the sum in the operator $\mathcal{Q}$ extends over all permutations P of the standard ordering $1, 2, \ldots, N$ of the set of electron space and spin coordinates. The Slater determinants of order N constructed from the single-particle states $\phi_{k_i}(i)$ which are the solutions of Eq. (6) form an antisymmetic, orthonormal, and complete set of eignefunctions.[11]

The Schrödinger equation for the unperturbed system of atom plus radiation field is

$$(H_{\text{atom}} + H_{\text{rad}}) \phi_{k_1 \cdots k_N} \psi_{\cdots n_\omega \cdots}$$

$$= E_{k_1 \cdots k_N \cdots n_\omega \cdots} \phi_{k_1 \cdots k_N} \psi_{\cdots n_\omega \cdots} , \quad (8)$$

where

$$E_{k_1 \cdots k_N \cdots n_\omega \cdots} = \sum_{i=1}^{N} \epsilon_{k_i} + \sum_{\omega} n_\omega \hbar \omega . \quad (9)$$

The ground state of our noninteracting system (8) is approximated by $\phi_{k_i \cdots k_n \cdots} \psi_{\cdots n_\omega \cdots}$, where the N electrons are distributed among the single-particle states $k_1, k_2, \ldots, k_N$ which are ordered so that the most tightly bound state is k_1, the next k_2, etc., until all N single-particle states are populated sequentially, and in $\psi_{\cdots n_\omega \cdots}$, all the n_ω's are zero. Excited states $\phi_{l_1 \cdots l_n \cdots} \psi_{\cdots n'_\omega \cdots}$ are obtained by promoting any number of electrons from the occupied states $k_1, k_2, \ldots, k_N$ to unoccupied states l_j, and by populating the radiation field with the desired number n'_ω of photons of a given description. (In actuality, in forming excited states of the system, the maximum number of promoted electrons will be two, and the number of photons either zero or one.)

The above is the starting point for the calculation of radiation processes, and transitions from one state of the atom to another result from the interaction H_I [Eq. (5)] between the atom and

radiation field. The transition probability for any given radiation process, whether simple emission or absorption or a more complicated process, can be obtained readily.[9] However, before calculating the radiative-Auger rate, we first consider how the usual radiative[13,14] and radiationless[14] transitions involving deep core levels can be obtained in this framework.

1. Radiative transitions

In the ordinary radiative transition, a deep inner-shell vacancy $(n_0 l_0)$ is filled by a less tightly bound electron (nl) and the liberated energy is carried away by an emitted photon [Fig. 1(a)].

The initial state $|i0_\omega\rangle$ which describes the excited atom and unexcited radiation field can be written

$$|i0_\omega\rangle = \mathcal{C}(\phi_{k_1}(1)\cdots\phi_{nl}(t)\cdots\phi_{k_N}(N))\psi_{0_\omega}, \quad (10)$$

and the final state $|f,1_\omega\rangle$, which describes the deexcited atom and excited radiation field, is

$$|f,1_\omega\rangle = \mathcal{C}(\phi_{m_1}(1)\cdots\phi_{n_0 l_0}(t)\cdots\phi_{m_N}(N))\psi_{1_\omega}. \quad (11)$$

(In the wave function describing the radiation field we have set all the n_ω's equal to zero except those describing the photon of interest, in which case n_ω is either 0_ω or 1_ω.) The matrix element of the interaction H_I[Eq. (5)] between the inital and final states given by Eqs. (10) and (11) reduces to

$$\langle m_1(1)\cdots n_0 l_0(t)\cdots m_N(N),1_\omega|\sum_{i=1}^{N}\mathcal{K}_i(\vec{A})\sqrt{N!}\ \mathcal{C}|\ k_1(1)\cdots nl(t)\cdots k_N(N)0_\omega\rangle. \quad (12)$$

In obtaining (12), we have made use of the fact that H_I commutes with the antisymmetrization operator $\mathcal{C}$, $\mathcal{C}^2 = \sqrt{N!}\,\mathcal{C}$,[12] and the terms in the interaction H_I which do not depend on the electromagnetic potential vanish between states differing by the number of quanta present in the radiation field. The matrix element (12) vanishes for final-state wave functions which differ by more than one single-particle state. Consequently, in this approximation, all the remaining $N-1$ electrons remain in their single-particle orbits. Expression (12) reduces to $\langle n_0 l_0 1_\omega|\mathcal{K}(\vec{A})|nl0_\omega\rangle$, so that the spontaneous emission transition rate in first order of perturbation theory is given by the familiar expression[9]

$$W_{nl\to n_0 l_0} = (2\pi/\hbar)|\langle n_0 l_0, 1_\omega|\mathcal{K}(\vec{A})|nl, 0_\omega\rangle|^2 \rho(E_f), \quad (13)$$

where $\rho(E_f)$ is the density of final states available to the emitted photon, whose energy, according to Eq. (9), is $\hbar\omega = \epsilon_{nl} - \epsilon_{n_0 l_0}$.

2. Radiationless transitions

Similarly, we can consider nonradiative or Auger transitions in the above framework. In a nonradiative transition, a vacancy in the $n_0 l_0$ inner shell is filled by an electron from the nl orbit, and simultaneously, an electron is excited from orbit $n'l'$ to $\epsilon\bar{l}$, typically in the continuum [Fig. 1(b)]. In this case the initial state of the atom and radiation field is described by $|i0_\omega\rangle$, where

$$|i0_\omega\rangle$$

$$= \mathcal{C}(\phi_{k_1}(1)\cdots\phi_{nl}(p)\cdots\phi_{n'l'}(q)\cdots\phi_{k_N}(N))\psi_{0_\omega}, \quad (14)$$

and the final state, since no photon is emitted, by

$$|f0_\omega\rangle$$

$$= \mathcal{C}(\phi_{m_1}(1)\cdots\phi_{n_0 l_0}(p)\cdots\phi_{\epsilon\bar{l}}(q)\cdots\phi_{m_N}(N))\psi_{0_\omega}. \quad (15)$$

Because of the orthogonality of the single-particle wave functions used to construct the Slater determinants, the only final states (15) which give nonvanishing matrix elements of the interaction H_I [Eq. (5)] are those that differ from the initial state (14) by the two-particle states involving electrons p and q. The terms in H_I involving single-particle operators or the electromagnetic potential vanish by the same arguments as above. The terms that survive are

$$\langle f0_\omega|H_I|i0_\omega\rangle = \langle n_0 l_0 \epsilon\bar{l}|(e^2/r_{12})|nln'l'\rangle$$
$$- \langle n_0 l_0 \epsilon\bar{l}|(e^2/r_{12})|n'l'nl\rangle. \quad (16)$$

If we denote the right-hand side of Eq. (16) by

$$\langle n_0 l_0 \epsilon\bar{l}|(e^2/r_{12})|nln'l'\rangle_A,$$

we get the Auger transition rate in first order of perturbation theory[14]:

$$W_{n_0 l_0 \to nl, n'l'}$$

$$= (2\pi/\hbar)|\langle n_0 l_0 \epsilon\bar{l}|(e^2/r_{12})|nln'l'\rangle_A|^2\rho(E_f), \quad (17)$$

where $\rho(E_f)$ is the density of final states available to the ejected Auger electron of energy $\epsilon = E_f$, and again from Eq. (9), $E_f \equiv \epsilon = \epsilon_{nl} + \epsilon_{n'l'} - \epsilon_{n_0 l_0}$. In this approximation, the electrons not participating directly in the transition remain in their single-particle orbits. Equation (17) is known as

Wentzel's ansatz[15,16] and is the starting point for calculations of nonradiative transition rates.[14]

After a radiationless transition fills the single inner-shell vacancy, the atom is left doubly ionized in the inner shells. The states of such nearly-closed-shell configurations with two holes can be expressed in terms of completely-closed-shell configurations together with the correlated two-electron configurations.[14,17] In LS coupling, the electrostatic energies are the same for the two systems. The initial and final states can therefore be represented by the two-electron configurations correlated to two-hole configurations that consist (initially) of one inner-shell vacancy and one hole in the continuum and (finally) of two inner-shell vacancies. In LS coupling, for an appropriately normalized electron continuum wave function, the total transition probability into all possible states of L and S for a given configuration of the atom is[18]

$$W = \sum_{L,S} \frac{(2S+1)(2L+1)}{2(2l_0+1)}$$

$$\times \sum_{T} \left| \frac{1}{\hbar} \langle n_0 l_0, \epsilon \bar{l}; SL \,|\, (e^2/r_{12}) \,|\, nl, n'l'; SL \rangle \right|^2 .$$

(18)

3. Radiative-Auger transitions

We consider radiative-Auger transitions in free atoms, and restrict ourselves to cases where a single inner-shell vacancy results in the excitation of an electron and emission of a photon. Specifically, we consider processes involving electrons initially in single-particle states nl and $n'l'$ and finally in $n_0 l_0$ (initial vacancy) and $n_f l_f$ (either bound or in the continuum) accompanied by an emitted photon [Fig. 1(c)]. The initial and final states of the atom plus radiation field are

given by

$$|i0_\omega\rangle = \mathcal{C}(\phi_{k_1}(1)\cdots\phi_{nl}(p)$$
$$\cdots\phi_{n'l'}(q)\cdots\phi_{k_N}(N))\psi_{0_\omega},$$
(19)

$$|f1_\omega\rangle = \mathcal{C}(\phi_{m_1}(1)\cdots\phi_{n_0 l_0}(p)$$
$$\cdots\phi_{n_f l_f}(q)\cdots\phi_{m_N}(N))\psi_{1_\omega}.$$

(20)

The matrix element of the perturbation H_I [Eq. (5)] evaluated between such unperturbed states of the entire system vanishes in first order. In second order of perturbation theory, the transition rate is[9]

$$W_{fi} = \frac{2\pi}{\hbar} \left| \sum_{n,n'_\omega} \frac{\langle f1_\omega | H_I | nn'_\omega\rangle\langle nn'_\omega | H_I | i0_\omega\rangle}{E_n - E_i} \right|^2$$

$$\times \delta(E_f - E_i),$$
(21)

where n and n'_ω are summed (or integrated) over all intermediate or virtual states, and E_n, E_i, and E_f are the unperturbed energies of the entire system in the intermediate, initial, and final states, respectively. The summation indices n and n'_ω in Eq. (21) denote different intermediate states of the system for which the N electrons populate single-particle states $n_1,\ldots,n_N$, and the radiation field is characterized by the presence of $\cdots n'_\omega \cdots$ photons of each description. The intermediate states $|nn'_\omega\rangle$ which will give nonvanishing matrix elements are of the form

$$|nn'_\omega\rangle = \mathcal{C}(\phi_{n_1}(1)\cdots\phi_{n_p}(p)\cdots\phi_{n_q}(q)\cdots\phi_{n_N}(N))\psi_{n'_\omega},$$

(22)

where $\psi_{n'_\omega}$ has the same meaning as in the above discussion of radiative transitions. The matrix element $\langle nn'_\omega | H_I | i0_\omega\rangle$ is then

$$\langle n_1(1)\cdots n_p(p)\cdots n_q(q)\cdots n_N(N); n'_\omega | \left(\sum_{i<j}^{N} \frac{e^2}{r_{ij}} - \sum_{i}^{N} V^N(r_i) \right.$$

$$\left. + \sum_{i} \mathcal{H}_i(\vec{A}) \right) \sqrt{N!}\, \mathcal{C} \,|\, k_1(1)\cdots nl(p)\cdots n'l'(q)\cdots k_N(N); 0_\omega\rangle .$$

(23)

In (23) the only terms that survive are those that involve intermediate states with the bra that are identical to the initial state or differ from it by only one- and two-particle states. Expression (23) then reduces to

$$\langle nn'_\omega | H_I | i0_\omega\rangle \approx \langle n_p n_q | (e^2/r_{pq}) | nln'l'\rangle_A \delta_{n'_\omega,0} \quad \{n_p \ne (nl), n_q \ne (n'l')\} + \langle n_p n'_\omega | \mathcal{H}_p(\vec{A}) | nl0_\omega\rangle \delta_{n_q,(n'l')}\{n_p \ne (nl)\}$$

$$+ \langle n_q n'_\omega | \mathcal{H}_q(\vec{A}) | n'l'0_\omega\rangle \delta_{n_p,(nl)}\{n_q \ne (n'l')\},$$

(24)

provided we make use of the following:

$$\sum_{n_j}^{occ} \langle n_j n_p | (e^2/r_{12}) | n_j k_p \rangle_A \approx \langle n_p | V^N | k_p \rangle . \quad (25)$$

In calculations of the ground-state energy of an atom,

$$\sum_{n_j}^{occ} \langle n_j n_p | (e^2/r_{12}) | n_j k_p \rangle_A = \langle n_p | V^N | k_p \rangle \quad (26)$$

defines the Hartree-Fock potential.[19] In our case we do not take the Hartree-Fock approach directly, since it is not designed to provide a complete, orthogonal set of functions such as that given by the Slater determinants constructed from the single-particle states of the model Hamiltonian (4). Nevertheless, the approximation given by Eq. (25) formally amounts to the Hartree-Fock

approach, and we can therefore choose for V^N the Hartree-Fock potential, or a single-particle potential which approximates the Hartree-Fock potential. This potential can then be used to generate single-particle states from which *all* the required many-particle wave functions (Slater determinants) are constructed.

Evaluation of $\langle f1_\omega | H_I | nn'_\omega \rangle$ yields an expression similar to (24), which multiplied by (24), divided by the energy denominator $E_n - E_i$, and summed over all intermediate photon states n'_ω results in the following expression for the radiative-Auger transition rate:

$$W_{fi} = (2\pi/\hbar) W(n_0 l_0, n_f l_f, 1_\omega; nl, n'l', 0_\omega) \delta(E_i - E_f) , \quad (27)$$

where

$$W[n_0 l_0, n_f l_f, 1_\omega; nl, n'l', 0_\omega] = \left| \sum_{\substack{n_p \neq (n_0 l_0), (n_f l_f) \\ n_q}}^{UO} \frac{\langle n_0 l_0 n_f l_f | (e^2/r_{12}) | n_p n_q \rangle_A \langle n_p n_q 1_\omega | \sum_{i=1}^2 \mathcal{H}_i(\vec{A}) | nln'l'0_\omega \rangle}{\epsilon_p + \epsilon_q + \hbar\omega - \epsilon_{nl} - \epsilon_{n'l'}} \right.$$

$$\left. + \sum_{\substack{n_p \neq (nl), (n'l') \\ n_q}}^{UO} \frac{\langle n_0 l_0 n_f l_f 1_\omega | \sum_{i=1}^2 \mathcal{H}_i(\vec{A}) | n_p n_q 0_\omega \rangle \langle n_p n_q | (e^2/r_{12}) | nln'l' \rangle_A}{\epsilon_p + \epsilon_q - \epsilon_{n'l'} - \epsilon_{nl}} \right|^2 . \quad (28)$$

The summations in (28) extend over all unoccupied single-particle states to which the electrons are promoted, with the unavailable states as noted. This expression for the radiative-Auger rate has the following interpretation: Consider first one of the terms in the first summation in Eq. (28); an electron in one of the initial single-particle states interacts with the electromagnetic field and makes a transition to an intermediate state, where it interacts with the other electron (still in the initial single-particle state) via the Coulomb interaction. As a result of this interaction, one electron jumps to $n_0 l_0$ (the initial vacancy) and the other to $n_f l_f$ (the final single-particle state of an excited electron) and the process is accompanied by the emission of a photon of energy $\hbar\omega$. The direct and exchange processes representing terms in the first summation in (28) are shown schematically in Figs. 2(a) and 2(b). Similarly, the terms in the second summation represent two electrons initially in the single-particle states nl and $n'l'$ which interact via the Coulomb interaction, one electron scattering to an intermediate state, the other to, say, $n_0 l_0$. The electron in the intermediate state interacts with the electromagnetic field and makes a transition to $n_f l_f$. The process is again accompanied by the emission of a photon of energy $\hbar\omega$. The direct and exchange processes are shown schematically in Figs. 2(c) and 2(d).

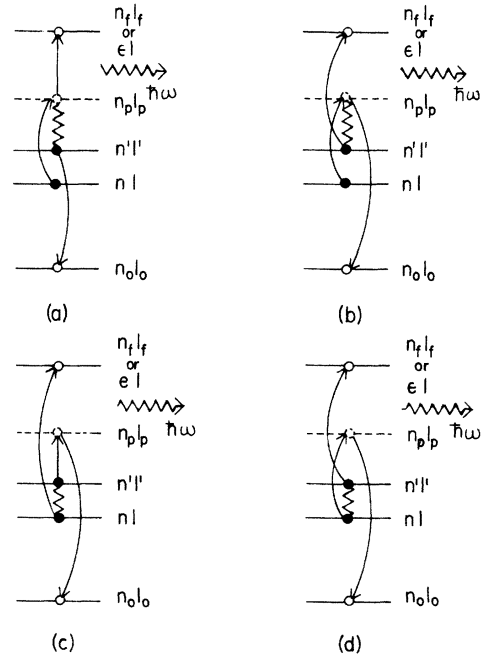The square of the sum of all the terms partially

FIG. 2. Schematic representation of the various terms in the expression for the radiative-Auger transition rate [Eqs. (27) and (28)]. (a) and (b) correspond to the direct and exchange terms, respectively, in the first sum of Eq. (28), (c) and (d) to direct and exchange terms in the second sum. The wavy line represents the Coulomb interaction between electrons, and $n_p l_p$ designate the quantum numbers of the intermediate state.

represented in Fig. 2 (between initial and final states of the system that satisfy conservation of energy) is shown in Fig. 1(c), and corresponds to the radiative-Auger process. In this approach, just as for radiative and nonradiative transitions discussed above, the electrons not participating directly remain in their single-particle orbits.

In order to get the transition probability per unit time, Eq. (27) has to be multiplied by the number of states per unit energy interval $\rho(E_i)$ available to the system and integrated over all energies E_i. The number of states dN is $\rho(E_i)\,dE_i$, and this

can also be written as $dN = dN_e\,dN_\omega$, by analogy with β decay,[20] where dN_e and dN_ω are the number of states available to the emitted electron and photon, respectively. Now dN_e and dN_ω are given by $\rho_e(E_e)\,dE_e$ and $\rho_\omega(\hbar\omega)\,d(\hbar\omega)$, where ρ_ω and ρ_e are the number of states per unit energy available to the emitted photon and excited electron. Thus

$$\delta(E_f - E_i)\,\rho(E_i)\,dE_i = \delta(E_{n_0 l_0} + \epsilon + \hbar\omega - \epsilon_{nl} - \epsilon_{n'l'})$$

$$\times \rho_e(\epsilon)\rho_\omega(\hbar\omega)\,d\epsilon\,d(\hbar\omega)\,, \qquad (29)$$

and the transition probability W_{fi} is

$$W_{fi} = \frac{2\pi}{\hbar} \sum_{n_f l_f} W(n_0 l_0, n_f l_f, 1_\omega; nl, n'l', 0_\omega)\rho_\omega(\epsilon_{nl} + \epsilon_{n'l'} - \epsilon_{n_0 l_0} - \epsilon_{n_f l_f})$$

$$+ \sum_{l_f} \int_0^{\epsilon_{nl} + \epsilon_{n'l'} - \epsilon_{n_0 l_0}} W(n_0 l_0, n_f l_f, 1_\omega; nl, n'l', 0_\omega)\rho_\omega(\epsilon_{nl} + \epsilon_{n'l'} - \epsilon_{n_0 l_0} - \epsilon)\rho_e(\epsilon)\,d\epsilon\,. \qquad (30)$$

To obtain Eq. (30) we have made use of the relationship

$$\int_0^\infty \int_0^\infty f(x)g(y)\,\delta(c - x - y)\,dx\,dy = \int_0^c f(x)g(c - x)\,dx\,,$$

which can be verified using the Heaviside function representation of the Dirac δ function.[21]

The first sum in Eq. (30) represents transitions of an electron to bound states of the atom, and the second sum represents transitions to the continuum.

In order to calculate the radiative-Auger rate explicitly, we proceed as in the Auger case discussed above, and evaluate the matrix elements in Eq. (28) between antisymmetrized and properly normalized two-particle wave functions of total angular momentum J and projection M. In the *LSJM* representation, the transition rate from an initial two-electron state of total momentum J_0, orbital angular momentum L_0, and spin S_0 to a final two-electron state of J, L, and S is obtained by replacing

$$W(n_0 l_0, n_f l_f, 1_\omega; nl, n'l', 0_\omega)$$

in Eq. (30) by

$$W(n_0 l_0, n_f l_f, SLJM; 1_\omega \,|\, nl, n'l', S_0 L_0 J_0 M_0; 0_\omega)\,,$$

where

$$W(n_0 l_0, n_f l_f, SLJM; 1_\omega \,|\, nl, n'l', S_0 L_0 J_0 M_0; 0_\omega)$$

$$= \frac{1}{4} \left| \sum_{\substack{n_p l_p, n_q l_q \neq n_0 l_0, n_f l_f \\ L' S' J' M'}}^{UO, nl, n'l'} \langle n_0 l_0 n_f l_f LSJM \,|\, (e^2/r_{12}) \,|\, n_p l_p n_q l_q L'S'J'M' \rangle \right.$$

$$\times \frac{\langle n_p l_p n_q l_q L'S'J'M'; 1_\omega \,|\, \sum_{i=1}^2 \mathcal{K}_i(\vec{A}) \,|\, nln'l' L_0 S_0 J_0 M_0; 0_\omega \rangle}{\epsilon_{n_p l_p} + \epsilon_{n_q l_q} + \hbar\omega - \epsilon_{n'l'} - \epsilon_{nl}}$$

$$+ \sum_{\substack{n_p l_p, n_q l_q \neq nl, n'l' \\ L' S' J' M'}}^{UO, n_0 l_0 n_f l_f} \langle n_0 l_0 n_f l_f LSJM; 1_\omega \,|\, \sum_{i=1}^2 \mathcal{K}_i(\vec{A}) \,|\, n_p l_p n_q l_q L'S'J'M'; 0_\omega \rangle$$

$$\left. \times \frac{\langle n_p l_p n_q l_q L'S'M' \,|\, (e^2/r_{12}) \,|\, nln'l' L_0 S_0 J_0 M_0 \rangle}{\epsilon_{n_p l_p} + \epsilon_{n_q l_q} - \epsilon_{n'l'} - \epsilon_{nl}} \right|^2\,. \qquad (31)$$

The matrix elements of both the Coulomb and $\vec{p} \cdot \vec{A}$ interaction are evaluated between antisymmetrized two-particle states of total angular momentum J and projection M. The total radiative-Auger transition rate into all final states of the system is obtained by summing Eq. (30) [with the replacement (31)] over all projections of angular momenta involved, over all L and S (commensurate with J) as well as the J of the atom allowed by angular momentum selection rules, and averaging over initial states of the system.

C. Comparison with previous descriptions of the radiative-Auger process

We consider next the comparison of the present approach with previous descriptions of the radiative-Auger process. As discussed above, there exist, at present, only two calculations of the total radiative-Auger transition rate,[6,7] both of which are based on the sudden approximation. In what follows, we compare the present calculation with the more recent, systematic, and more complete work of Åberg.[6]

If we let $\phi_i(x_1, \ldots, x_N)$ describe the initial single-vacancy state, and $\psi_f(x_1, \ldots, x_N)$ the final single- or double-vacancy core plus excited electron state, then Eq. (1) of Ref. 6 and Eq. (1) of this paper follow directly from the general expression for the transition rate:

$$W_{fi} = \frac{2\pi}{\hbar} \left| (\psi_f \Phi_{1_\omega} | \frac{e}{mc} \sum_{i=1}^{N} \vec{p}_i \cdot \vec{A}(\vec{r}_i) | \phi_i \Phi_{0_\omega}) \right|^2 \rho(E_f) . \tag{32}$$

The functions ψ_f, ϕ_i, and Φ_{n_ω} have the same interpretation as given following Eq. (8), and in Åberg's work,[6] ϕ_i and ψ_f are N-particle Slater determinants constructed from single-particle states obtained by solving the separate SCF equations for the initial $(n_0 l_0)^{-1}$, single-hole, and final $[(nl)^{-1}(n'l')^{-1}]\epsilon\bar{l}$ and $(nl)^{-1}$ configurations. In the sudden approximation, the eigenfunctions ϕ_i of the initial Hamiltonian are related to the eigenfunctions ψ_f of the final Hamiltonian at the instant the perturbation is turned on by[22]

$$\phi_i = \sum_m (\psi_m | \phi_i) \psi_m , \tag{33}$$

where

$$(\psi_m | \phi_i) = \int \psi_m^*(x_1, \ldots, x_N) \phi_i(x_1, \ldots, x_N) \, dx_1 \cdots dx_N .$$

(The initial and final Hamiltonians describe an atom with one initial and one or two final vacancies, respectively.) The matrix element in (32) can be written $(\psi_f \Phi_{1_\omega} | H_I | \phi_i \Phi_{0_\omega})$, where H_I is given by Eq. (5), since the matrix elements of the Coulomb interaction and the single-particle potential $V^N(r_i)$ vanish between wave functions which involve a change in the number of quanta present in the radiation field. Substituting ϕ_i [Eq. (33)] into the matrix element $(\psi_f \Phi_{1_\omega} | H_I | \phi_i \Phi_{0_\omega})$ gives

$$(\psi_f \Phi_{1_\omega} | H_I | \phi_i \Phi_{0_\omega})$$

$$= \sum_{m, n_\omega} (\psi_m \Phi_{n_\omega} | \phi_i \Phi_{0_\omega})(\psi_f \Phi_{1_\omega} | H_I | \psi_m \phi_{n_\omega}) . \tag{34}$$

In obtaining Eq. (34) we have to remember that we are treating the atom and radiation field as one system. If we then approximate $\phi_i \Phi_{0_\omega}$ by

$$\phi_i \Phi_{0_\omega} \approx \psi_i \Phi_{0_\omega} + \sum_{l, n'_\omega} \frac{(\psi_i \Phi_{n'_\omega} | H_I | \psi_i \Phi_{0_\omega}) \psi_l \Phi_{n'_\omega}}{E_{i, 0_\omega} - E_{l, n'_\omega}} , \tag{35}$$

that is, if we expand the initial state (which is an eigenfunction of the initial Hamiltonian of the entire system) in terms of the eigenfunctions of the final Hamiltonian of the entire system to first order in perturbation theory, then for ψ_m's and $\Phi_{n'_\omega}$'s individually orthonormal,

$$(\psi_m \Phi_{n_\omega} | \phi_i \Phi_{0_\omega}) = \delta_{m, i} \, \delta_{n_\omega, 0} + \frac{(\psi_m \Phi_{n_\omega} | H_I | \psi_i \Phi_{0_\omega})}{E_{i, 0_\omega} - E_{m, n_\omega}} . \tag{36}$$

It follows immediately that

$$(\psi_f \Phi_{1_\omega} | H_I | \phi_i \Phi_{0_\omega})$$

$$= (\psi_f \Phi_{1_\omega} | H_I | \psi_i \Phi_{0_\omega})$$

$$+ \sum_{m, n_\omega} \frac{(\psi_f \Phi_{1_\omega} | H_I | \psi_m \Phi_{n_\omega})(\psi_m \Phi_{n_\omega} | H_I | \psi_i \Phi_{0_\omega})}{E_{i, 0_\omega} - E_{m, n_\omega}} . \tag{37}$$

The first term in Eq. (37) vanishes by the same arguments presented in Sec. II B. Substituting (37) into (32) leads directly to Eq. (21), the expression for the transition rate in second order. This rather sketchy derivation shows that Eqs. (32) and (21) are the same if one assumes that Eq. (35) holds. The latter expresses the initial state of the system in terms of wave functions which are eigenfunctions of the final or fully relaxed system and considers, at least to first order, interactions between all the electrons and the electromagnetic field. Thus in the above sense the present approach and the approach based on the sudden approximation are theoretically equivalent.

With Eq. (21) as starting point in the present approach, and the condition that excited (and intermediate) states of the atom can be constructed from single-particle states of a model Hamiltonian, it follows that the electrons not participating directly in the transition remain in their single-particle orbits and serve only to generate the field in which the participants interact. That one need consider only correlations between the two participating electrons greatly simplifies the problem and enables one to calculate the spectral distribution of the emitted photon, something not readily done with Eqs. (1) or (32) as starting points.

III. *K-MM* RADIATIVE-AUGER TRANSITION RATE IN ARGON

A. Wave functions

In this section we calculate the *K-MM* radiative-Auger rate in the argon atom. Although there exist a number of spectra in the literature in which the structure on the low-energy side of emission lines is attributed to the radiative-Auger process,[1-5] we chose the experimental *K* radiative-Auger spectrum of argon[5] as a test of our approach and calculations because of its apparent complexity of features.

In order to evaluate the *K-MM* radiative-Auger transition rate in the free argon atom according to Eqs. (30) and (31), some appropriate choice of single-particle wave functions is required, i.e., a choice of $V^N(r_i)$ has to be made in our model Hamiltonian (4). According to the discussion in Sec. III B, the appropriate choice of potential is a Hartree-Fock potential or one that generates single-particle wave functions that are quite similar to those obtained from a Hartree-Fock potential.

We have calculated the radiative-Auger transition rates for bound states using screened hydrogenic wave functions and corresponding energies[18] in a preliminary check of Eq. (30). It was observed that while the matrix elements involved were somewhat sensitive to variations in the wave functions (via the effective charge), the transition rate and obviously the position of the lines were very sensitive to the single-particle energies used. Since a large number of wave functions and single-particle energies are required, speed of computation is an important factor. In order to verify our approach and compare the calculation with the experiment, we have chosen to calculate the transition rate with single-particle wave functions determined by a one-electron potential in an Ar⁺ ion obtained from a scaled Thomas-Fermi (STF) ionic charge distribution[23] where the scale factors are chosen to make the one-electron binding energies agree with experimental ionization potentials. [The introduction of the scale factor corresponds to a uniform dilation and contraction of the Thomas-Fermi (TF) charge distribution which compensates

for all the omissions and approximations of the TF model.]

K and *M* binding energies for neutral argon[24] and tabulated experimental Ar⁺ and Ar⁺⁺ energy values,[25,26] together with some Ar autoionization data of Ogurtsov *et al.*,[5,28] were used to determine the scale factors in the STF ionic charge distribution. In those instances where experimental energy values were not available, e.g., the $(3s)^{-1}(3p)^{-1}nl$ Ar⁺ configuration, energies were extrapolated from tabulated Ar and Ar⁺⁺ energies[24-26] (energies with asterisks in column 3 of Table I). (The STF wave functions for the neutral argon atom agree very well with Hartree-Fock wave functions.[27] The 3s and 3p STF functions showed deviations from the calculated Hartree-Fock functions very similar to those shown in Fig. 3 of Ref. 23 for neutral krypton.) Using these wave functions, the $K\beta_{1,3}$ emission rate $(K-M_2$ and $K-M_3)$ in argon is found to be 0.0067 eV/$\hbar$ compared to 0.0054 eV/$\hbar$ calculated with the relativistic Hartree-Slater theory.[29]

The bound- and continuum-state radial wave functions $R_{nl}(r) = P_{nl}(r)/r$, calculated in the STF field, satisfied the usual normalization conditions[23]:

$$\int_0^\infty P_{nl}^2(r)\, dr = 1, \quad \text{if } \epsilon_{nl} < 0,$$

$$P(r) \xrightarrow[r\to\infty]{} \cos[kr + \delta(r)], \quad \text{if } \hbar^2 k^2/2m > 0.$$
(38)

Enclosing the atom in a large spherical volume of radius R_0 that tends to infinity, the requirement that the wave function must vanish on the boundary $r = R_0$ results in a density of states per unit energy interval $\rho_e(\epsilon)$ for the ejected electron given by

$$\rho_e(\epsilon) = \frac{2}{\pi} \left(\frac{2m}{\hbar^2} \right)^{1/2} \frac{1}{\sqrt{\epsilon}},$$

where ϵ is the electron's energy and m is its mass.

B. Evaluation of the matrix elements

The matrix elements of both the Coulomb and $\vec{p}\cdot\vec{A}$ interaction were evaluated between antisymmetrized, normalized two-particle wave functions, which in the *LSJM* representation are of the form[30]

$$\psi_A(n_a l_a, n_b l_b; SLJM) = \sum_{M_L M_S} (SM_S LM_L | JM)[\phi(n_a l_a, n_b l_b LM_L) + (-1)^{l_a + l_b - L + S}\phi(n_b l_b, n_a l_a LM_L)]X(\tfrac{1}{2}\tfrac{1}{2}SM_S),$$
(39)

where

$$\phi(n_\alpha l_\alpha, n_\beta l_\beta LM_L) = \sum_{m_\alpha m_\beta} (l_\alpha m_\alpha l_\beta m_\beta | LM_L)\, \phi_1(l_\alpha m_\alpha)$$
$$\times \phi_2(l_\beta m_\beta) R_1(n_\alpha l_\alpha) R_2(n_\beta l_\beta),$$
(40)

$$X(\tfrac{1}{2}\tfrac{1}{2}SM_S) = \sum_{m_S m_S'} (\tfrac{1}{2}m_S \tfrac{1}{2}m_S' | SM_S) X_1(m_S) X_2(m_S'),$$
(41)

and $\phi_i(l_j m_j)$, $R_i(n_j l_j)$, and $X_i(m_S')$ are the single-particle angular, radial, and spin wave functions

of electron i with quantum numbers n_j, l_j, m_j, and m'_s.

The evaluation of the $\vec{p} \cdot \vec{A}$ matrix element in Eq. (31) using the wave functions (39) gives rise to four terms, each of the type

$$\langle n_\alpha l_\alpha n_\beta l_\beta L M_L; 1_\omega \mid \sum_i \mathcal{K}_i(\vec{A}) \mid n_\gamma l_\gamma n_\delta l_\delta L' M'_L 0_\omega \rangle,$$

where $\mid n_\alpha l_\alpha n_\beta l_\beta L M_L 0_\omega \rangle$ is a product of Eq. (34) and the function describing the radiation field. These matrix elements can be calculated most conveniently be expanding the vector potential $\vec{A}$ of the electromagnetic field in $\mathcal{K}_i(\vec{A})$ [Eq. (3)], in a series of standing spherical waves about the origin of a sphere of radius r_0.[31] For dipole radiation the matrix element of $\mathcal{K}_i(\vec{A})$ between single-particle

states,

$$\langle n_\sigma l_\sigma m_\sigma 1_\omega \mid \mathcal{K}(\vec{A}) \mid n_\rho l_\rho m_\rho 0_\omega \rangle,$$

is given by

$$\langle n_\sigma l_\sigma m_\sigma 1_\omega \mid \mathcal{K}(\vec{A}) \mid n_\rho l_\rho m_\rho 0_\omega \rangle$$

$$= e\left(\frac{8\pi\omega}{9r_0\hbar c^2}\right)^{1/2} (\epsilon_{n_\sigma l_\sigma} - \epsilon_{n_\rho l_\rho}) \sum_{\mu=-1}^{1} \langle n_\sigma l_\sigma m_\sigma \mid r Y_1^\mu \mid n_\rho l_\rho m_\rho \rangle,$$

$$(42)$$

and the density of states per unit energy interval available to the emitted photon, $\rho_\omega(\hbar\omega)$, is $r_0/\pi\hbar c$.[31] After some algebra, the matrix element of the $\vec{p} \cdot \vec{A}$ interaction in Eq. (31) becomes

$$\langle n_a l_a n_b l_b SLJM; 1_\omega \mid \sum_{i=1}^{2} \mathcal{K}_i(\vec{A}) \mid n_c l_c n_d l_d S'L'J'M'; 0_\omega \rangle$$

$$= e\left(\frac{8\pi\omega}{9r_0\hbar c^2}\right)^{1/2} \delta_{SS'}[(2J+1)(2J'+1)(2L+1)(2L'+1)]^{1/2}(-1)^{-M} \begin{Bmatrix} 1 & J' & J \\ S & L & L' \end{Bmatrix} \sum_\mu \begin{pmatrix} 1 & J' & J \\ \mu & M' & -M \end{pmatrix}$$

$$\times \Bigg(\delta_{n_a, n_c} \delta_{l_a, l_c} (-1)^{l_a + l_d + L + L'} \begin{Bmatrix} L & L' & 1 \\ l_d & l_b & l_a \end{Bmatrix} (\epsilon_{n_a l_a} - \epsilon_{n_d l_d}) \langle n_b l_b \| r \| n_d l_d \rangle \langle l_b \| Y_1 \| l_d \rangle$$

$$+ \delta_{n_a, n_d} \delta_{l_a, l_d} (-1)^{L+S'} \begin{Bmatrix} L & L' & 1 \\ l_c & l_b & l_a \end{Bmatrix} (\epsilon_{n_b l_b} - \epsilon_{n_c l_c}) \langle n_b l_b \| r \| n_c l_c \rangle \langle l_b \| Y_1 \| l_c \rangle$$

$$+ \delta_{n_b, n_c} \delta_{l_b, l_c} (-1)^{l_a + l_d + L' + S'} \begin{Bmatrix} L & L' & 1 \\ l_d & l_a & l_b \end{Bmatrix} (\epsilon_{n_a l_a} - \epsilon_{n_d l_d}) \langle n_a l_a \| r \| n_d l_d \rangle \langle l_a \| Y_1 \| l_d \rangle$$

$$+ \delta_{n_b, n_d} \delta_{l_b, l_d} (-1)^{l_a + l_b} \begin{Bmatrix} L & L' & 1 \\ l_c & l_a & l_b \end{Bmatrix} (\epsilon_{n_a l_a} - \epsilon_{n_c l_c}) \langle n_a l_a \| r \| n_c l_c \rangle \langle l_a \| Y_1 \| l_c \rangle \Bigg), \qquad (43)$$

where

$$\begin{Bmatrix} l_1 & l_2 & l_3 \\ m_1 & m_2 & m_3 \end{Bmatrix} \quad \text{and} \quad \begin{Bmatrix} j_1 & j_2 & j_3 \\ l_1 & l_2 & l_3 \end{Bmatrix}$$

are the Wigner 3-j and Racah 6-j symbols,[30] respectively, and $\langle \alpha \| C \| \beta \rangle$ denotes the reduced matrix element of the operator C.[30]

The evaluation of the Coulomb matrix elements in Eq. (31) follows along similar lines. The Coulomb interaction potential is expressed in terms of a scalar product of irreducible-tensor operators,[30]

$$\frac{1}{r_{12}} = \sum_{\nu,\mu} \gamma_\nu(r_1, r_2) C_{\nu\mu}^*(\Omega_1) C_{\nu\mu}(\Omega_2),$$

where

$$\gamma_\nu = \begin{cases} r_1^\nu/r_2^{\nu+1}, & r_1 < r_2, \\ r_2^\nu/r_1^{\nu+1}, & r_2 < r_1, \end{cases} \qquad C_{\nu\mu} = \left(\frac{4\pi}{2\nu+1}\right)^{1/2} Y_\nu^\mu(\Omega), \qquad (44)$$

and the Y_ν^μ's are the spherical harmonics. Straightforward angular momentum algebra yields

$$\langle n_a l_a n_b l_b LSJM \, | \, (e^2/r_{12}) \, | \, n_c l_c n_d l_d L'S'J'M' \rangle$$

$$= e^2 (-1)^{l_b+l_d+L} \left(\sum_\nu F_\nu(n_a l_a, n_b l_b, n_c l_c, n_d l_d, L) + (-1)^{-L+S} \, G_\nu(n_a l_a, n_b l_b, n_c l_c, n_d l_d, L) \right) \delta_{SS'} \delta_{LL'} \delta_{JJ'} \delta_{MM'}, \qquad (45a)$$

where

$$F_\nu(n_a l_a, n_b l_b, n_c l_c, n_d l_d, L) = \langle l_a \| C_\nu \| l_c \rangle \langle l_b \| C_\nu \| l_d \rangle \begin{Bmatrix} l_a & l_b & L \\ l_d & l_c & \nu \end{Bmatrix} \{ (n_a l_a) \, | \, (n_c l_c), (n_b l_b), \nu, (n_d l_d) \}, \qquad (45b)$$

$$G_\nu(n_a l_a, n_b l_b, n_c l_c, n_d l_d, L) = F_\nu(n_a l_a, n_b l_b, n_d l_d, n_c l_c, L). \qquad (45c)$$

Following the notation of Ref. 14, the radial matrix elements are denoted by

$$\{ (n_\alpha l_\alpha) \, | \, (n_\beta l_\beta), (n_\gamma l_\gamma), p, (n_\delta l_\delta) \} = \int_0^\infty r_1^2 \, dr_1 \int_0^\infty \gamma_p(r_1, r_2) R_{n_\alpha l_\alpha}(r_1) R_{n_\delta l_\delta}(r_2) R_{n_\beta l_\beta}(r_2) R_{n_\gamma l_\gamma}(r_2) r_2^2 \, dr_2. \qquad (46)$$

C. *K-MM* radiative-Auger transitions in Argon

. If we examine expression (31) and replace $\hbar\omega$ in the denominator of the first series of terms by

$$\hbar\omega = \epsilon_{nl} + \epsilon_{n'l'} - \epsilon_{n_0 l_0} - \epsilon_{n_f l_f},$$

which follows from conservation of energy in the transition, the denominator becomes

$$\epsilon_{n_r l_r} + \epsilon_{n_s l_s} - \epsilon_{n_0 l_0} - \epsilon_{n_f l_f}.$$

The matrix element of the $\vec{p} \cdot \vec{A}$ interaction, [Eq. (43)] gives rise to energy differences $\epsilon_{n_\alpha l_\alpha} - \epsilon_{n_p l_p}$ in the numerator, and since the values $n_0 l_0$ and $n_f l_f$ are excluded from the intermediate states in this case, the typically large single-particle energy $\epsilon_{n_0 l_0}$ (K binding energy) which appears in the denominator does not appear in the numerator (This is not true for the second summation, in which the $n_0 l_0$ and $n_f l_f$ values are not excluded from $n_r l_r$ and $n_s l_s$, and $\epsilon_{n_0 l_0}$ can appear simultaneously in the numerator and denominator.) Since the K binding energy is always appreciably greater than the binding or excitation energies of the other electrons involved, one would expect the magnitude of the first sum in Eq. (31) to be smaller than that of the second sum, and hence the major strength of

the radiative K-MM Auger transition due to the latter. That this is not unreasonable can be seen from Fig. 2. Figures 2(a) and 2(b) depict the Coulomb interaction between an electron in one of the initial single-particle states and an electron in some intermediate state $n_r l_r$ to which it has been promoted following its interaction with the electromagnetic field. One would expect this process to be much weaker than the one shown in Figs. 2(c) and 2(d), where electrons in very similar orbits first interact via the Coulomb interaction, a situation analogous to the dominant first-order Auger process.

In light of the above, we have neglected in the present calculation of the K-MM radiative-Auger rate the first summation in Eq. (31). Substituting Eqs. (43) and (45) into Eq. (31), and neglecting the first summation, we find that the *total* radiative-Auger rate from an initial state of the atom with a K vacancy to a final state of an atom involving two vacancies in the $3l$ and $3l'$ levels, an electron promoted to $n_f l_f$ (a bound or continuum level of the atom), and an emitted photon of energy

$$\hbar\omega = \epsilon_{3l} + \epsilon_{3l'} - \epsilon_{n_f l_f} - \epsilon_{1s}$$

is, in atomic units,

$$W = \frac{4\alpha^3}{3} \sum_{L,S} (2L+1) \left(\sum_{n_f l_f} E_\omega(\epsilon_{3l} + \epsilon_{3l'} - \epsilon_{n_f l_f} - \epsilon_{1s}) W(1s, n_f l_f, SL \, | \, 3l3l'S_0 L_0) \right.$$

$$\left. + \sum_{l_f} \frac{\sqrt{2}}{\pi} \int_0^{\epsilon_{3l}+\epsilon_{3l'}-\epsilon_{1s}} E_\omega(\epsilon_{3l} + \epsilon_{3l'} - \epsilon_{1s} - \epsilon_f) W(1s, \epsilon_f l_f SL \, | \, 3l3l'S_0 L_0) \frac{d\epsilon_f}{(\epsilon_f)^{1/2}} \right), \qquad (47)$$

where

$$W(1s, n_f l_f, LS \mid 3l, 3l'SL_0) = \left| \sum_{n_p, l_p, \sigma} \begin{Bmatrix} L & L_0 & 1 \\ l_p & 0 & l_f \end{Bmatrix} (\epsilon_{1s} - \epsilon_{n_p l_p}) \langle 1s \| r \| n_p l_p \rangle \langle 0 \| C_1 \| l_p \rangle \right.$$

$$\times \frac{F_\sigma(n_p l_p, n_f l_f, 3l, 3l', L) + (-1)^{-L_0 + S} G_\sigma(n_p l_p, n_f l_f, 3l, 3l', L)}{\epsilon_{n_p l_p} + \epsilon_{n_f l_f} - \epsilon_{3l} - \epsilon_{3l'}}$$

$$+ \sum_{n_p l_p \sigma} \begin{Bmatrix} L & L_0 & 1 \\ l_p & l_f & 0 \end{Bmatrix} (\epsilon_{n_f l_f} - \epsilon_{n_p l_p}) \langle n_f l_f \| r \| n_p l_p \rangle \langle l_f \| C_1 \| l_p \rangle$$

$$\times \left. \frac{F_\sigma(n_p l_p, 1s, 3l, 3l', L) + (-1)^{-L_0 + S} G_\sigma(n_p l_p, 1s, 3l, 3l', L)}{\epsilon_{n_p l_p} + \epsilon_{1s} - \epsilon_{3l} - \epsilon_{3l'}} \right|^2. \tag{48}$$

The summation over $n_p l_p$ in Eq. (48) extends over the same values as in the second sum in Eq. (31), and the F_σ and G_σ factors are given by Eqs. (45b) and (45c).

The transition rate W [Eq. (47)] was evaluated numerically for argon on a PDP-10 computer, with the only input data being the nl and nl' of the M shell and the single-particle binding energies of the electrons involved (see Sec. III A). Wigner 3-j and Racah 6-j computer subroutines[32] selected the possible final- and intermediate-state electron angular momenta, as well as the possible final L and S values of the atom, and calculated the appropriate angular factors. All radial matrix elements were evaluated numerically with STF wave functions generated by another computer subroutine based on Ref. 23.

In evaluating W [Eq. (47)], it was found that the major contribution to the transition rate occurs when the intermediate states $n_r l_r$ are the same as nl or $n'l'$, the initial single-particle states of the electrons, a result similar to that observed by Bloch.[7] Furthermore, the total rate did not change appreciably when the summation over intermediate states contained bound states beyond $8f$ or continuum states, and hence the summation over these states was terminated at $8f$.

IV. RESULTS AND DISCUSSION

A. Radiative K-MM Auger transition rate and spectral distribution of emitted photons

In Table I we present the calculated transition rate for transitions in which an electron is excited into a bound state of the argon ion by the K-MM radiative-Auger process. The first column shows possible final configurations of atom and excited electron with principal quantum numbers n up to $n = 7$. The energies of these transitions relative to the $K\beta_{1,3}(\epsilon_{3p} - \epsilon_{1s})$ line are shown in column 3. These were obtained either directly from optical data[25,26] or estimated (entries followed by asterisk).

The calculated partial transition rates per unit energy interval for electrons excited to continuum

states, evaluated at a number of energies of the ejected electron, are shown in Table II. The energies of the continuum thresholds, relative to the $K\beta_{1,3}$ line, which are shown in column 4 were obtained from Ref. 5 and are based on experimental L_3MM Auger energies[28] and Ar L_3 and M_3 binding energies.[33] The more intense rates are plotted versus energy in Fig. 3, with the discrete transition rates converted to transition rates per unit energy interval owing to the finite lifetime broadening of the initial level.

The effect of the finite lifetime of the K vacancy is included by convoluting a Lorentzian line shape whose width is that of the K level with the calculated transition rate. The K-level width in argon (0.656 eV) was taken as the sum of the calculated radiationless,[18] radiative, and radiative-Auger widths, with the last two calculated using STF wave functions. The intensity and width of the calculated $K\beta_{1,3}$ line are shown for comparison. The resulting spectral distribution of the emitted photon (transition rate per unit energy interval versus energy), which is the sum over the individual contributions shown in Tables I and II, is shown in Fig. 4(a).

The total K-MM radiative-Auger transition rate, summed over the possible contributions from transitions to bound states and integrated over contributions to excited states in the continuum, is given in Table III. The total K-MM radiative-Auger rate is 2.68×10^{-4} eV$/\hbar$, or 4% of the calculated $K\beta_{1,3}$ rate of 6.7×10^{-3} eV$/\hbar$.

B. Comparison with experiment

We compare our calculated results with the experimental data of Keski-Rahkonen and Utriainen,[5] who measured the K-MM radiative-Auger spectrum in argon gas with a single-crystal LiF spectrometer whose horizontal divergence was limited by a Soller collimator.[34]

Keski-Rahkonen and Utriainen associated the various features in the spectrum [dots in Fig. 4(b)] labeled A, B, ... with transitions from the initial

$(1s)^{-1}\,^2S$ state of the atom to the following $K\text{-}M^2$ final-state multiplets:

$$((3p)^{-2},\ ^3P,\ ^1D,\ ^1S)mp \quad \text{or} \quad \epsilon p\,^2P^o;$$

$$((3s)^{-1}(3p)^{-1},\ ^3P,\ ^1P)ms,nd, \quad \text{or} \quad \epsilon s,\epsilon d\,^2P^o;$$

$$((3s)^{-2}\,^1S)mp \quad \text{or} \quad \epsilon p\,^2P^o.$$

On the basis of energies of these multiplets, ob-

TABLE I. Calculated partial *K-MM* radiative-Auger transition rates in argon for an electron excited into different bound states of the argon ion. The energies of the *K-MM* radiative-Auger lines (relative to the $K\beta_{1,3}$ line) either were obtained directly or were estimated (entries followed by asterisk) from optical data, Refs. 25 and 26. The notation $A\ (n)$ means $A\times10^n$.

Final-state configuration	Transition probability (eV/$\hbar$)	Energy shift from $K\beta_{1,3}$ (eV)
$(3p)^{-2}\,^3P$ $4p$ $P_{3/2,\,1/2}$	0.378 (−4)	−19.9
5p	0.114 (−4)	−23.6
6p	0.035 (−4)	−25.2
7p	0.006 (−4)	−25.9
$(3p)^{-2}\,^1D$ $4p$ $P_{3/2,\,1/2}$	0.926 (−5)	−21.4
5p	0.286 (−5)	−23.6
6p	0.007 (−5)	−25.3*
7p	0.002 (−5)	−26.1*
$(3p)^{-2}\,^1S$ $4p$ $P_{3/2,1/2}$	0.250 (−5)	−23.8
5p	0.072 (−5)	−26.9*
6p	0.002 (−5)	−27.8*
7p	<10⁻⁹	−28.6*
$(3p)^{-2}\,^1D$ $4f$ $P_{3/2,\,1/2}$	0.097 (−7)	−25.9
5f	0.112 (−7)	−27.2*
6f	0.122 (−7)	−27.7*
7f	0.063 (−7)	−28.5*
$(3s)^{-2}\,^1S$ $4p$ $P_{3/2,1/2}$	0.738 (−7)	−48.2
5p	0.251 (−7)	−51.2
6p	0.019 (−7)	−52.2
7p	0.006 (−7)	−53.0
$(3s)^{-1}(3p)^{-1}\,^1P$ $3d$ $P_{3/2,1/2}$	0.393 (−5)	−36.2
4d	0.045 (−5)	−40.5
5d	0.018 (−5)	−42.3
6d	0.011 (−5)	−44.2*
$(3s)^{-1}(3p)^{-1}\,^1P$ $4s$ $P_{3/2,\,1/2}$	0.325 (−6)	−33.3
5s	0.175 (−6)	−39.1
6s	0.007 (−6)	−41.2
7s	<10⁻⁹	−41.6*
$(3s)^{-1}(3p)^{-1}\,^3P$ $3d$ $P_{3/2,\,1/2}$	0.468 (−5)	−32.6
4d	0.083 (−5)	−36.9
5d	0.043 (−5)	−38.7
6d	0.010 (−5)	−39.3
$(3s)^{-1}(3p)^{-1}\,^3P$ $4s$ $P_{3/2,1/2}$	0.112 (−5)	−30.1
5s	0.057 (−5)	−36.5
6s	0.005 (−5)	−38.6
7s	0.002 (−5)	−39.6

tained from optical data and measured *L-MM* Auger energies, the peak A is assigned to the discrete transition

$$(1S)^{-1}\,^2S \to ((3p)^{-2},\ ^3P,\ ^1D)4p\,^2P^{o,}$$

and peak B to

$$(1S)^{-1}\,^2S \to ((3p)^{-2},\ ^1S)4p\,^2P$$

$$((3p)^{-2},\ ^3P,\ ^1D,\ ^1S)mp\,^2P^o.$$

The threshold energies for the continua are expected to begin somewhere in the valley between peaks B and C. The feature C is thought to consist of contributions from transitions to both the continuum and discrete states, with the main contribution from discrete $(1s)^{-1}\,^2S \to ((3s)^{-1}(3p)^{-1}$, $^3P,\ ^1P)ms$ or $nd\,^2P^o$ transitions. Finally, the features D and E are interpreted as the onset of the $(1s)^{-1}\,^2S \to (3s)^{-1}(3p)^{-1}\epsilon s$, $\epsilon d\,^2P^o$continua.

On the basis of our calculated partial rates [Fig. 3 (as well as Tables I and II)] we find that we completely agree with this interpretation of the *K-MM* radiative-Auger spectrum. We find, however, that the main contribution from discrete transitions to the feature C occurs from $(1S)^{-1}\,^2S \to ((3s)^{-1}(3p)^{-1}\,^3P,\ ^1P)\ 3d\,^2P^o$ transitions only, the $((3s)^{-1}(3p)^{-1}\,^3P,P)ms$ transitions being quite weak.

In order to compare our calculated photon spectrum [Fig. 4(a)] with the experimental spectrum [dots in Fig. 4(b)], the effect of the spectrometer window function on the former has to be included (or, alternately, the experimental spectrum corrected for instrumental effects). If $S(\epsilon)$ is the calculated (or unmodified) spectral distribution plotted against photon energy ϵ, e.g., Fig. 4(a), then the observed distribution at a spectrometer energy $\bar{\epsilon}$ is
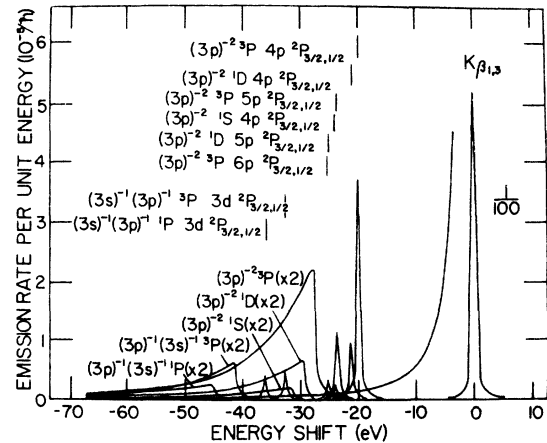

FIG. 3. Calculated major *K* −*MM* radiative-Auger photon emission rates per unit energy interval in argon, including effects of *K*-level width.

$$S(\bar{\epsilon}) = \int_{-\infty}^{\infty} S(\epsilon) \, W(\bar{\epsilon}, \epsilon - \bar{\epsilon}) \, d\epsilon , \qquad (49)$$

where $W(\bar{\epsilon}, \epsilon - \bar{\epsilon})$ is the spectrometer window function.[35,36] The spectrometer window function in this case depends on the horizontal and vertical divergence of the beam incident on the analyzing-crystal as well as the energy of the radiation (Bragg angle). We have assumed a triangular window function $W(\bar{\epsilon}, \epsilon - \bar{\epsilon})$ whose base is given by $\Delta\bar{\epsilon} = 2\bar{\epsilon}(\alpha + \frac{1}{4}\phi^2 \tan\theta)\cot\theta$ (Ref. 36), where α is the horizontal divergence, ϕ is the vertical divergence, and θ is the Bragg angle corresponding to energy $\bar{\epsilon}$. To simplify calculations of $S(\bar{\epsilon})$ according to Eq. (49) using the $S(\epsilon)$ given in Fig. 4(a),

we take $\Delta\bar{\epsilon}$ to be constant (energy independent) and corresponding to a value at the midpoint of the energy range of interest (3.110–3.190 keV). The horizontal beam divergence in the experiment determines α,[5] and the energy of the radiation, together with the $2d$ spacing of LiF (4.0173 Å), determine θ. Since no vertical divergence is quoted in Ref. 5, we take $\phi = 0$. The resulting geometrical-window-corrected spectrum is shown in Fig. 4(b) (continuous curve). The experimental data[5] (dots) and the above window-corrected calculated K-MM spectrum (continuous curve) are overdrawn on the same energy scale with the experimental $K\beta_{1,3}$ peak normalized to the calculated

TABLE II. Calculated partial K-MM radiative-Auger transition rates in argon per unit energy interval for an electron excited into the continuum. Energies of the continua thresholds (relative to the $K\beta_{1,3}$ line) were obtained from Ref. 5.

Final-state configuration	Energy of excited electron (eV)	Transition probability $(1/\hbar)$	Threshold shift from $K\beta_{1,3}$ (eV)
$(3p)^{-2}\,^3P$	1.4	0.121 (−4)	−27.6
	8.2	0.048 (−4)	
	16.3	0.021 (−4)	
	27.2	0.008 (−4)	
	43.5	0.002 (−4)	
	136.0	0.793 (−7)	
$(3p)^{-2}\,^1D$	1.4	0.282 (−5)	−29.4
	8.2	0.120 (−5)	
	16.3	0.051 (−5)	
	27.2	0.019 (−5)	
	43.5	0.008 (−5)	
	136.0	0.765 (−8)	
$(3p)^{-2}\,^1S$	1.4	0.852 (−6)	−31.6
	8.2	0.356 (−6)	
	16.3	0.149 (−6)	
	27.2	0.056 (−6)	
	43.5	0.016 (−6)	
	136.0	0.290 (−9)	
$(3s)^{-2}\,^1S$	1.4	0.412 (−7)	−54.7
	8.2	0.226 (−7)	
	16.3	0.116 (−7)	
	27.2	0.050 (−7)	
	43.5	0.016 (−7)	
	136.0	0.218 (−12)	
$(3s)^{-1}(3p)^{-1}\,^3P$	1.4	0.256 (−8)	−41.5
	8.2	0.101 (−8)	
	16.3	0.040 (−8)	
	27.2	0.014 (−8)	
	43.5	0.004 (−8)	
	136.0	0.111 (−9)	
$(3s)^{-1}(3p)^{-1}\,^1P$	1.4	0.110 (−5)	−45.3
	8.2	0.058 (−5)	
	16.3	0.026 (−5)	
	27.2	0.010 (−5)	
	43.5	0.002 (−5)	
	136.0	0.373 (−9)	

TABLE III. Total K-MM radiative-Auger transition rates in $(10^{-4}$ eV/$\hbar)$ in argon into different final-state configurations. n denotes bound and ϵ continuum electron states.

Final-state configuration	Transition probability
$(3p)^{-2}\,{}^{3}P\ np\ P_{1/2,\,3/2}$	0.436
$(3p)^{-2}\,{}^{1}D\ np\ P_{1/2,3/2}$	0.122
$(3p)^{-2}\,{}^{1}S\ np\ P_{1/2,3/2}$	0.033
$(3p)^{-2}\,{}^{1}D\ nf\ P_{1/2,3/2}$	0.002
$(3s)^{-2}\,{}^{1}S\ np\ P_{1/2,3/2}$	0.001
$(3s)^{-1}(3p)^{-1}\,{}^{3}P\ nd\ P_{1/2,3/2}$	0.061
$(3s)^{-1}(3p)^{-1}\,{}^{3}P\ ns\ P_{1/2,3/2}$	0.017
$(3s)^{-1}(3p)^{-1}\,{}^{1}P\ nd\ P_{1/2,3/2}$	0.047
$(3s)^{-1}(3p)^{-1}\,{}^{1}P\ ns\ P_{1/2,3/2}$	0.005
Total bound	0.725
$(3p)^{-2}\,{}^{3}P\ \epsilon p$	1.130
$(3p)^{-2}\,{}^{1}D\ \epsilon p,\ \epsilon f$	0.320
$(3p)^{-2}\,{}^{1}S\ \epsilon p$	0.093
$(3s)^{-2}\,{}^{1}S\ \epsilon p$	0.005
$(3s)^{-1}(3p)^{-1}\,{}^{3}P\epsilon d,\ \epsilon s$	0.121
$(3s)^{-1}(3p)^{-1}\,{}^{1}P\ \epsilon d,\ \epsilon s$	0.287
Total continuum	1.956
Total	2.681

$K\beta_{1,3}$ peak.

If we compare our instrumental-window-corrected spectrum (continuous curve) with the experimental data (dots) in Fig. 4(b), we find that qualitatively the overall spectral features can be reproduced quite well, the only major difference between the two being the apparent foreshortening of the calculated spectrum. A detailed comparison of theory and experiment is hampered by the lack of knowledge of the exact form of the spectrometer window function and experimental conditions under which the data were recorded.

The effect of the window function on the experimental spectrum is somewhat difficult to ascertain. First of all, the width of the window function is not constant but changes with energy by a factor of 2 over the energy range of interest. Thus the simplifying assumption of a constant-width window function evaluated at the midpoint of the energy range tends to underestimate this width at higher energies and overestimate it at lower energies. The effect of such an energy-independent window function on the spectrum in Fig. 4(a) is to enhance the height of the "corrected" higher-energy peaks such as peak A [Fig. 4(b), continuous curve] and depress and smear out lower-energy peaks, peaks D and E. Second, the effects due to vertical di-
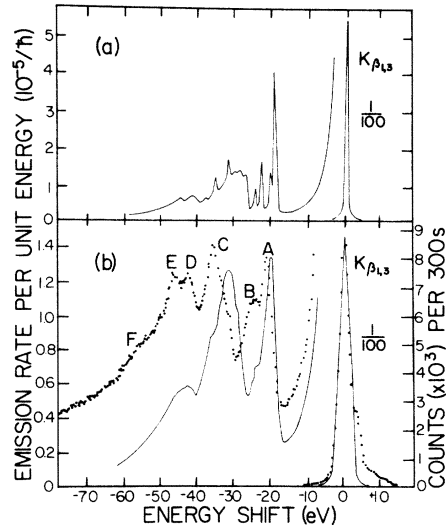

FIG. 4. (a) Calculated photon spectral distribution emitted in the K —MM radiative-Auger process in free argon. (b) Above spectral distribution modified by triangular spectrometer window function of angular divergence quoted in Ref. 5 (solid line), together with measured distribution (dots). Latter redrawn from Ref. 5, and experimental $K\beta_{1,3}$ line intensity normalized to calculated $K\beta_{1,3}$ line intensity.

vergence are not negligible. Vertical divergence tends to draw out the low-energy side of the spectrometer window function.[36] Although the extent of vertical beam divergence is not given in Ref. 5, a spread of 1°, not unreasonable for a typical single-crystal spectrometer arrangement, broadens the base of the window function by an amount comparable to the width of the K level in argon (0.66 eV).

Among the experimental details not discussed in Ref. 5 is the presence or absence of background radiation. Since the fluorescence spectrum was induced by x rays generated by a chromium anode operated at 50 kV and 36 mA,[5] a considerable amount of continuous radiation must have been present. It seems to us therefore that an appreciable amount of scattered, or directly incident on the crystal, bremsstrahlung radiation was unavoidably passed along with the radiation of interest at each spectrometer setting. That there was some background radiation can be inferred from the general appearance of the experimental spectrum at low energies [Fig. 1 of Ref. 5, and same spectrum redrawn in Fig. 4(b) (dots) of this paper]. An estimated constant background count rate of 3 counts/sec, subtracted from the experimental data, modifies the spectrum in the direction that tends to improve the agreement between theory and experiment.

The above discussion illustrates some of the difficulties which preclude a more detailed comparison of the calculated and experimental spectra, and points to the definite need for higher-resolution data. [A factor of 3 or so in resolving power $(\lambda/\Delta\lambda \sim 5000)$ in the data of Keski-Rahkonen and Utriainen would have greatly simplified the comparison between theory and experiment.] Consequently, it is somewhat difficult at this point to reach any definite conclusions regarding some of the specific differences between the experimental and window-corrected calculated spectrum [especially on the low-energy side of feature C in Fig. 4(b), since it is not clear if the observed discrepancies are due to an overestimation of the width of the spectrometer window function, the neglect of the first sum in Eq. (31), or both].

The calculated total K-MM radiative-Auger rate, which is 4% of the calculated $K\beta_{1,3}$ emission rate, agrees quite well with the experimentally observed ratio of radiative-Auger to $K\beta_{1,3}$ intensity of 0.05 (no error quoted). Shakeoff and configuration interaction predict 7.3%.[6]

V. CONCLUSION

In conclusion, we feel that our calculation, which is the first detailed calculation of the spectral distribution of photons emitted in the radiative-Auger process, reproduces the major portion of the K radiative-Auger spectrum in argon, and offers some detailed insight into the nature of the radiative-Auger process. The calculation is in a sense still preliminary, and a number of points have to be investigated further. These include the use of other wave functions, the effects of neglecting some of the terms in the expression for the transition rate, and the truncation of the summation and integration over intermediate states. The investigation of these points, together with a more complete calculation of the K-MM radiative-Auger process in a number of elements based on the above above approach, is currently in progress. (Preliminary results, using single-particle energies and wave functions obtained from solutions of a Hamiltonian with a Hartree-Fock-Slater potential, indicate that none of the major conclusions will have to be changed.)

In our calculation of the radiative-Auger transition rate we used wave functions that approximated the fully relaxed Ar^+ ion and Ar^+ experimental excitation energies. While the matrix elements in the transition rate are, relatively speaking, not too sensitive to the wave functions, the calculation is very sensitive to the single-particle energies used, and single-particle energies other than those of a fully relaxed Ar^+ ion (obtained from experimental data) lead to spectra vastly different from that shown in Fig. 4(a). Thus core relaxation plays a very important role in the calculation of the radiative-Auger process, an observation also noted by Åberg.[6]

On the experimental side, we feel that there is definite need for higher-resolution data on the radiative-Auger process in argon. As discussed in Sec. IV B, the comparison between theory and experiment in the present case has been greatly hampered by the unknown shape of the spectrometer response functions, the effect of which on the observed spectrum is decidedly not negligible.

The reasonable success in reproducing at least qualitatively the general form of the radiative-Auger spectrum in this case points to the potential use of the radiative-Auger process in the investigation of unoccupied bound states of various systems, including highly excited ions produced in energetic ion-atom collisions, and atoms in aggregates. The latter would require fairly high-resolution emission spectra; such spectra can be readily obtained for any number of elements and compounds with the aid of intense synchrotron radiation sources in the x-ray region.

*Present address: Physics Dept., Pontificia Universidade Catolica do Rio de Janeiro, Rio de Janeiro, Brazil.

[1]F. Bloch and P. A. Ross, Phys. Rev. 47, 884 (1935).

[2]T. Åberg and J. Utriainen, Phys. Rev. Lett. 22, 1346 (1969).

[3]J. Siivola, J. Utriainen, M. Linkoaho, G. Graeffe, and T. Åberg, Phys. Lett. 32A, 438 (1970).

[4]J. W. Cooper and R. E. LaVilla, Phys. Rev. Lett. 25, 1745 (1970).

[5]O. Keski-Rahkonen and J. Utriainen, J. Phys. B 7, 55 (1974).

[6]T. Åberg, Phys. Rev. A 4, 1735 (1971).

[7]F. Bloch, Phys. Rev. 48, 187 (1935).

[8]F. K. Richtmyer, J. Franklin Inst. 208, 325 (1929).

[9]W. Heitler, *The Quantum Theory of Radiation* (Oxford U. P., Oxford, 1954), 3rd ed. Chap. IV.

[10]M. Wolfsberg and M. L. Perlman, Phys. Rev. 99, 1833 (1955).

[11]U. Fano and J. W. Cooper, Rev. Mod. Phys. 40, 441 (1968).

[12]H. A. Bethe, *Intermediate Quantum Mechanics* (Benjamin, New York, 1964), Chap. 6.

[13]See, e.g., J. H. Scofield, Phys. Rev. 179, 9 (1969).

[14]W. Bambynek, B. Crasemann, R. W. Fink, H. U. Freund, H. Mark, C. D. Swift, R. E. Price, and P. Venugopola Rao, Rev. Mod. Phys. 44, 716 (1972).

[15]G. Wentzel, Z. Phys. 43, 524 (1927).

[16]E. H. S. Burhop, *The Auger Effect* (Cambridge U. P., Cambridge, 1952), Chap. 2.

[17]W. N. Asaad and E. H. S. Burhop, Proc. Phys. Soc. Lond. 71, 369 (1958).

[18]V. O. Kostroun, M. H. Chen, and B. Crasemann, Phys. Rev. A 3, 533 (1971).

[19]R. Brout and P. Carruthers, *Lectures on the Many-Electron Problem* (Interscience, New York, 1963), Chap. 2.

[20]C. S. Wu and S. A. Moszkowski, *Beta Decay* (Wiley, New York, 1966), Chap. 1.

[21]A. Messiah, *Quantum Mechanics* (North-Holland, Amsterdam, 1961), p. 469.

[22]L. I. Shiff, *Quantum Mechanics*, 2nd ed. (McGraw-Hill, New York, 1955), p. 217.

[23]J. C. Stewart and M. Rotenberg, Phys. Rev. 140, A1508 (1965).

[24]J. F. Bearden and A. F. Burr, Rev. Mod. Phys. 39, 125 (1967).

[25]C. E. Moore, *Atomic Energy Levels* (Natl. Bur. Stand., U.S. GPO, Washington, D. C., 1949).

[26]L. Minnhagen, Ark. Fys. 25, 203 (1963).

[27]J. B. Mann, *Atomic Structure Calculations II; Hartree Fock Wavefunctions and Radial Expectation Values: Hydrogen to Lawrencium* (U.S. Department of Commerce, Springfield, Va., 1968), LA 3691.

[28]G. N. Ogurtsov, I. P. Flaks, and S. V. Avakyan, Zh. Eksp. Teor. Fiz. 57, 27 (1969) [Sov. Phys.-JETP 30, 16 (1970)].

[29]J. H. Scofield, Phys. Rev. 179, 9 (1969).

[30]A. deShalit and I. Talmi, *Nuclear Shell Theory* (Academic, New York, 1963).

[31]S. A. Moszkowski, *Theory of Multipole Radiation*, in *Alpha- Beta- and Gamma-Ray Spectroscopy*, edited by K. Siegbahn (North-Holland, Amsterdam, 1965), Vol. 2.

[32]Our formulas for these symbols are given by A. R. Edmonds, *Angular Momentum in Quantum Mechanics* (Princeton U. P., Princeton, 1957).

[33]K. Siegbahn *et al.*, *ESCA Applied to Free Molecules* (North-Holland, Amsterdam, 1969).

[34]W. Soller, Phys. Rev. 24, 158 (1924).

[35]J. S. Thomsen, in *X-Ray Spectroscopy*, edited by L. Azaroff (McGraw-Hill, New York, 1974), p. 31.

[36]L. G. Parratt, Special Notes on Experiment X-4, Cornell Advanced Physics Laboratory Course (Cornell Univ., 1955) (unpublished).